Proceedings RootS25
3rd International Workshop on Soil-Vegetation-Atmosphere Interaction
Boldrin D, Cecconi M, Cotecchia F, Leung A, Pedone G, Perrini P, Romero E, Tagarelli V, Zdravković L (eds)
ISSN: 3107-300X

doi: doi.org/10.53243/RootS2025-4

Root–soil interaction modelling for understanding tree anchorage mechanisms

Jun Zhu[1], Anthony Kwan Leung[1]*, Teing Teing Tan[1], Zhaoyi Wu[1]

[1] *State Key Laboratory of Climate Resilience for Coastal Cities, Department of Civil and Environmental Engineering, the Hong Kong University of Science and Technology, Hong Kong SAR*

ABSTRACT: Tree stability under wind mainly depends on the mechanical interactions between its root systems and surrounding soil. Numerical modelling offers an effective approach to evaluate tree root anchorage by performing virtual push-over tests on known root system architecture (RSA). However, prior models using embedded beam elements (EBE), while computationally efficient, assume unrealistically rigid root–soil bonding and neglect gaps or relative displacement between roots and soil. This simplification omits interfacial shearing and root pull-out failure, hindering accurate assessment of anchorage capacity and a deep understanding of root–soil interaction mechanisms. Recently, a root anchorage model has been introduced to employ a 3D frictional point-to-point contact formulation to capture root–soil interaction and load transfer at the interface. Building on this, this study used that model to investigate root overturning behaviour under lateral push-over. The model was validated against a centrifuge push-over test using a 3D-printed realistic RSA, accurately capturing maximum overturning resistance and post-peak response. Parametric simulations revealled substantial differences in overturning resistance across distinct push-over directions and identified root axial angle as the dominant factor governing the strength mobilisation of lateral roots upon push-over.

Keywords: Numerical modelling; Root–soil interaction; Root anchorage; Root system architecture; Tree stability

1 INTRODUCTION

Assessing root anchorage is essential for evaluating tree safety. Numerical approaches—especially finite-element (FE) method—offer a powerful tool to quantify anchorage capacity under diverse loading scenarios and to resolve the mobilisation of stresses within individual root members, thereby capturing root–soil interaction mechanisms. Previous studies have demonstrated that the embedded beam element (EBE) method can provide a computationally efficient way to capture axial tension, compression and bending behaviours of roots (Zhu et al. 2022). In this approach, complex root system architectures (RSAs) are discretised into straight beam elements that are kinematically coupled to the surrounding soil via an embedded constraint, so root displacements follow the interpolated soil displacement field (Yang et al. 2014). However, a key limitation of the EBE method is the lack of considering root–soil relative displacement. This limitatin prohibits the simulation of root–soil interface shearing and root pull-out failure (Zhu et al. 2025), hampering a deeper understanding of the mechanisms governing root–soil load transfer and the mobilisation of root resistance under lateral push-over.

This study implemented a recently developed root anchorage model (Zhu et al. 2024) within a FE framework to investigate the overturning behavior of realistic RSAs. The model was first validated against published centrifuge test data on tree push-over (Zhang et al. 2023) and then used to examine the mobilisation of root strength when the RSA was subjected to lateral push-over displacements applied from different directions.

2 ROOT ANCHORAGE MODEL

2.1 Root-soil mechanical interaction

The complex RSA was discretised by a network of interconnected beam elements. Zhu et al. (2024) developed a root anchorage model (i.e. RTS model) to capture the root–soil interaction. This model defines the contact pair at the integration point of deformed root element (i.e. reference point **R**) and the virtual point placed within the host soil element (i.e. target point **S**) at the same global coordinates as **R** (Fig. 1a). The relative displacement ($\boldsymbol{u}_{rel}$) between contact points **R** and **S** can be decomposed into one normal component ($\boldsymbol{u}_n$) and two tangential components. Their directions are determined following Ninić et al. (2014):

- First tangential direction $\tilde{\boldsymbol{t}}_1$: the vector connecting global coordinates of the root element's end nodes.
- Normal direction $\tilde{\boldsymbol{n}}$: projecting the point **R** onto an auxiliary plane orthogonal to $\tilde{\boldsymbol{t}}_1$, and connecting the point **R** to the projection point ($\boldsymbol{y}_s^{proj}$; Fig. 1(b))
- The second tangential direction $\tilde{\boldsymbol{t}}_2$: the cross product of $\tilde{\boldsymbol{t}}_1$ and $\tilde{\boldsymbol{n}}$ (i.e. $\tilde{\boldsymbol{t}}_2 = \tilde{\boldsymbol{t}}_1 \times \tilde{\boldsymbol{n}}$).

The contact stress components (p_n, p_{t1}, and p_{t2}) were calculated using a penalty formulation. The resultant tangential contact stress (p_t) is limited by the Coulomb's friction law:

$$p_t = \sqrt{p_{t1}^2 + p_{t2}^2} \le p_n \tan\delta, \quad (1)$$

where δ is the interface friction angle, which depends expotentially on the resultant shearing displacement ($\hat{u}_t = \|\boldsymbol{u}_{t1} + \boldsymbol{u}_{t2}\|$) as follows:

$$\delta = \delta_{cr} + (\delta_p - \delta_{cr})\exp[-\eta(\hat{u}_t - \hat{u}_t^0)], \quad (2)$$

where δ_p and δ_{cr} are the interface friction angles at the peak and critical states, respectively, and their values can be measured through interface constant-normal-load, direct-shear tests (Zhang et al. 2023); η is interface softening constant. $\hat{u}_t^0$ is the tangential displacement at the onset of debonding phase.

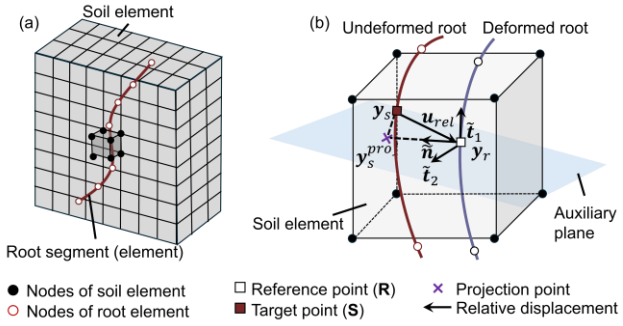

Figure 1. Illustration of the RTS model; (a) 1-D root (beam) element and 3-D soil (solid) element; and (b) definitions of the contact directions and the relative displacement components (after Zhu et al. 2024)

2.2 Root mechanical behaviour

An elastic-damage constitutive model (Linde et al. 2004) was adopted to capture the brittle behaviour of roots. In this model, a damage factor (f_b) is defined to indicate the onset of root breakage failure:

$$f_b = \sqrt{\frac{\varepsilon_r^t}{\varepsilon_r^c}(\varepsilon_r)^2 + \left(\varepsilon_r^t - \frac{(\varepsilon_r^t)^2}{\varepsilon_r^c}\right)\varepsilon_r}, \quad (3)$$

where ε_r is the mobilised root internal strain. ε_r^t and ε_r^c are the root ultimate tensile and compressive strains, respectively, which are determined by the ratio of their corresponding ultimate strength (i.e. σ_r^t and σ_r^c) to the elastic modulus E_r. An exponential function (D_{bf}) is also employed to describe the evolution of root damage:

$$D_{bf} = 1 - \frac{\varepsilon_r^t}{f_b}\exp\left(-\frac{E_r\varepsilon_r^t(f_b - \varepsilon_r^t)l_r}{G_b}\right), \quad (4)$$

where G_b is the breakage energy of the root material. Finally, the root internal stress (σ_r) can be expressed as:

$$\sigma_r = (1 - D_{bf})E_r\varepsilon_r. \quad (5)$$

2.3 Soil mechanical behaviour

An enhanced Mohr–Coulomb constitutive model grounded in critical state theory (EMC–CS) proposed by Zhu et al. (2024) was adopted to simulate the complex soil response during root–soil interaction. In contrast to the original Mohr–Coulomb model, which assumes perfectly elastic–perfectly plastic behavior, the EMC–CS model uses a simple exponential law, initially proposed by Doherty and Muir Wood (2013), to describe the mobilisation of the friction variable ($\mathbb{H} = \sin\phi'$, where ϕ' is the effective soil friction angle) with the plastic deviatoric strain (ε_J^p), as follows:

$$\varepsilon_J^p = \frac{\mathbb{H}}{\alpha(\mathbb{H}_p - \mathbb{H})} - \frac{\mathbb{H}_0}{\alpha(\mathbb{H}_p - \mathbb{H}_0)}, \quad (6)$$

where α is the controlling variable; $\mathbb{H}_0$ is the initial soil friction variable used to ensure $\varepsilon_J^p = 0$ when the initial yield surface is first intersected; $\mathbb{H}_p$ is the friction variable of the soil at the peak state. To account for soil strain-softening behaviour, a linear relationship between $\mathbb{H}_p$ and state paremeter (ψ) is incorporated into the EMC–CS model:

$$\mathbb{H}_p = \mathbb{H}_{cr}(1 - k_h\langle -\psi\rangle), \quad (7)$$

where k_h is the hardening constant; $\mathbb{H}_{cr}$ is the friction variable of the soil at the critical state. Soil's volumetric response is captured using a non-associated flow rule (i.e. Taylor's flow rule). Further details on the EMC–CS model, including mathematic derivations, parameter definitions, model implementation, and validation, are provided in Zhu et al. (2024).

3 MODEL VALIDATION

The root anchorage model that integrated the soil and root constitutive models and the root–soil interaction model (via user-defined element subroutine) was implemented into the ABAQUS/Explicit solver for the simulation of root anchorage behaviour. The model was first validated against a centrifuge push-over test on a complex *Pinus pinaster Ait.* RSA (Zhang et al. 2023) embedded in saturated sandy silt with a relative density of 45%–50%. The RSA was 3D-printed using ABS material based on the field excavation data from Danjon and Reubens (2008). The elastic modulus (E_r) and tensile strength (σ_r^t) of the root analogue were measured from three-point bending tests (Liang et al. 2015):

$$E_r = 7.28(d_r)^{-0.794}, \quad (8)$$

$$\sigma_r^t = 164.7(d_r)^{-0.52}. \quad (9)$$

Other key input parameters for root anchorage model used in both cases are summarised in Table 1. To minimise boundary influence, the FE domain comprised a 15 m × 15 m × 6 m soil block (Fig. 2a). The soil surrounding the roots was meshed with an average

element size of 0.4 m. The mesh dependency inherent to the strain-softening model was not addressed in the present study and will be examined in future work. The bottom of the soil domain was fixed to avoid any movements in both horizontal and vertical directions, whilst all the vertical boundaries were restrained from the lateral movements. A rigid, vertical trunk with height length of 2.4 m and constant diameter of 28.8 cm (Fig. 2b) was kinematically tied to the root stump so that the stump and trunk base shared the same displacement. A lateral displacement was applied at a height of 1.2 m above ground at a constant rate of 5 mm/s. In addition to the X+ push-over used in the centrifuge test, three further loading directions were considered in the simulations: X−, Y+, and Y− for comparisons.

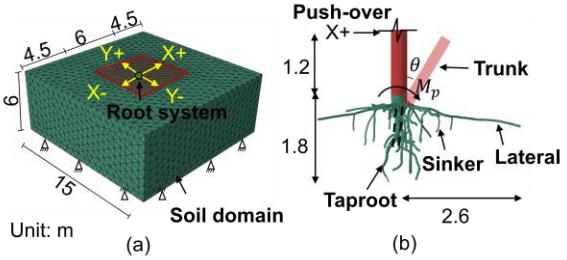

Figure 2. (a) FE mesh conditions; (b) RSA dimensions (after Zhu et al. 2024)

Table 1. Input parameters of root anchorage model

Parameters		Unit	Value
Γ	CSL constant	[–]	2.1
λ	CSL constant	[–]	0.115
G_0	Shear modulus constant	[–]	3300
β	Shear modulus exponent	[–]	0.4
υ	Poisson's ratio	[–]	0.4
Θ	Attraction component	[kPa]	0
$\mathbb{H}_{cr}$	Friction variable at the critical state	[–]	0.62
α_0	Fitting coefficients of α	[–]	151
α_1	Fitting coefficients of α	[–]	0
k_d	Dilatancy constant	[–]	1.5
k_h	Hardening constant	[–]	2.2
δ_p	Peak interface friction angle	[°]	38.7
δ_{cr}	Critical interface friction angle	[°]	27.6
η	Interface softening constant	[–]	100
t_s	Interface shear thickness	[mm]	0.72
G_b	Root breakage energy	[J/m^2]	1280

Figure 3 compares the measured and computed overturning moment–rotation ($M_p - \theta_p$) curves of the RSA under lateral push-over. Whilst some slight fluctuations were found, primarily due to numerical instability commonly encountered with penalty contact constraints, the significant drops in M_p were attributed to the continues breakages of root components. For reference, results from an EBE model (Yang et al. 2014) are also shown. Compared to the EBE model, the proposed root anchorage model markedly improved prediction of the peak overturning moment ($M_{p,max}$), reducing error up to 190%. It also successfully predicted the residual overturning resistance at large overturning rotation which was otherwise failed to be captured by the existing EBE model. The simulations further revealled evident directional dependence of anchorage behaviour, with differences in $M_{p,max}$ of up to 66% across different push-over directions, highlighting the strong influence of RSA anisotropy on anchorage performance.

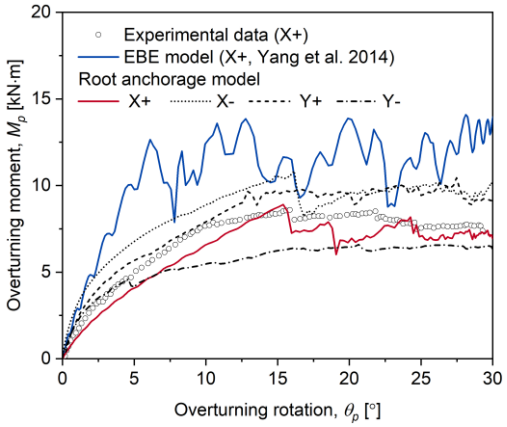

Figure 3. Comparisons of the measured and computed overturning moment-rotation curves in the push-over case

4 MOBILISATION OF ROOT STRENGTH

The back-analysis was used to improve the understanding of mobilisation of root strength and explain root anchorage mechanisms during overturning. A dimensionless variable, root utilisation (χ_r), was defined by normalising root internal stress (σ_r) with respect to root strength (σ_r^t), to capture the level of ultimate (i.e. breakage) strength of each individual root segment mobilised. A higher value of χ_r indicates a root closer to breakage. Root axial angle (Θ_r), which is the angle between the root segment centreline and the positive X-axis, was used to define the root segment orientation. Figure 4 presents the mobilisation of χ_r versus root axial angle (Θ_r) for both laterals (red) and sinkers (blue). Across all cases, lateral roots oriented approximately opposite to the push-over direction (e.g. within the range of 135°–225° in Fig 4a) mobilised higher root utilisation. Conversely, laterals more closely aligned with the push-over direction (e.g. within the range of 0°–45° and 315°–0° Fig 4a) exhibited much lower mobilisation of χ_r against overturning. These differences arise from distinct loading mechanisms. During overturning, root segments with small angular offsets to the loading direction intended to be pushed into the soils, experiencing mainly compression and bending; they were therefore more susceptible to buckling (Danquechin Dorval et al. 2016) and cannot fully mobilise their breakage strength. In contrast, segments oriented opposite to the loading direction were preferentially pulled out from the soil, experienced tension, and thus mobilised tensile capacity more

effectively to contribute to anchorage. These findings provide an important insight into root–soil interaction: axial orientation of segment relative to loading direction plays the dominant role in governing strength mobilisation of lateral roots for anchorage. By comparison, sinkers exhibited a more uniform distribution of χ_r across Θ_r in all four load cases, indicating a weaker association between χ_r and root axial orientation.

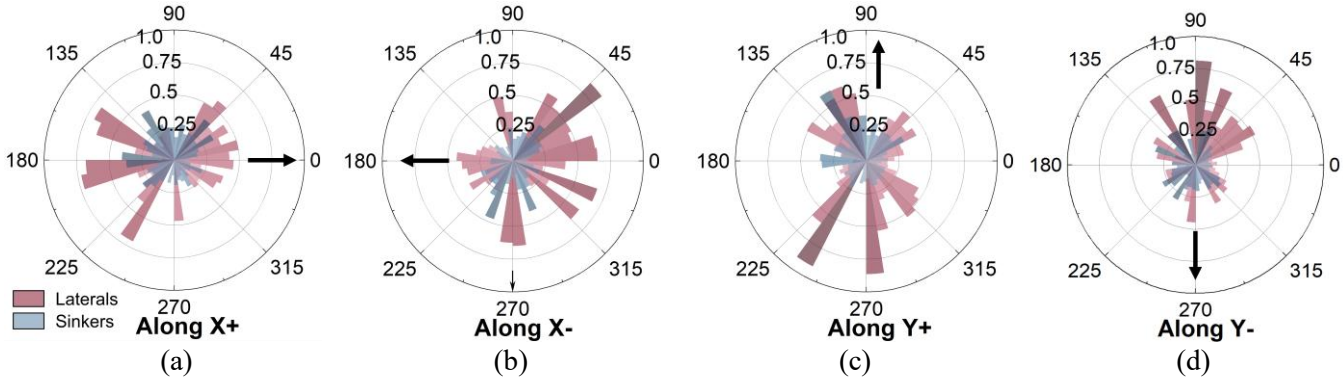

Figure 4. Mobilisation of root utilisation across root axial angle for lateral (red) and sinker (blue) roots under push-over loading applied along (a) X+, (b) X–, (c) Y+, and (d) Y– directions

5 CONCLUSION

This study utilised a recently developed numerical root anchorage model to investigate tree anchorage mecahnisms. The model was validated against a centrifuge push-over test of a complex RSA and was deomstrated to effectively reproduce both the anchorage capacity and the post-peak response. A parametric study identified substantial differences in root overturning resistance (up to 66%) for different lateral push-over directions, highlighting the strong influence of RSA anisotropy on anchorage performance. The back-analysis further revealed that for lateral roots, axial angle is the key factor governing the mobilisation of root breakage strength.

6 ACKNOWLEDGEMENTS

The authors thank the Hong Kong Research Grant Council (Grant Nos. GRF/16202422 and ITC-SJKCRCC26EG01) for the funding and the resources spent on this work. The authors are grateful to Dr. Frédéric Danjon of French National Institute for Agriculture, Food, and Environment (INRAE) for sharing the data source of the RSA of *Pinus pinaster Ait* for the analysis.

7 REFERENCES

Danjon, F., Reubens, B. 2008. Assessing and analyzing 3D architecture of woody root systems, a review of methods and applications in tree and soil stability, resource acquisition and allocation, *Plant and soil* **303**, 1–34.

Danquechin Dorval, A., Meredieu, C., Danjon, F. 2016. Anchorage failure of young trees in sandy soils is prevented by a rigid central part of the root system with various designs, *Annals of botany* **118**(4), 747–762.

Doherty, J.P., Muir Wood, D. 2013. An extended Mohr–Coulomb (EMC) model for predicting the settlement of shallow foundations on sand, *Géotechnique* **63**(8), 661–673.

Liang, T., Knappett, J.A., Leung, A., Carnaghan, A., Bengough, A G., Zhao, R. (2020). A critical evaluation of predictive models for rooted soil strength with application to predicting the seismic deformation of rooted slopes, *Landslides* **17**(1), 93–109.

Liang, T., Knappett, J.A., Duckett, N. 2015. Modelling the seismic performance of rooted slopes from individual root–soil interaction to global slope behaviour, *Géotechnique* **65**(12), 995–1009.

Linde, P., Pleitner, J., de Boer, H., Carmone, C. 2004. *Modelling and simulation of fibre metal laminates*. Paper presented at the ABAQUS Users' conference.

Ninić, J., Stascheit, J., Meschke, G. 2014. Beam–solid contact formulation for finite element analysis of pile–soil interaction with arbitrary discretization, *International Journal for Numerical and Analytical Methods in Geomechanics* **38**(14), 1453–1476.

Yang, M., Défossez, P., Danjon, F., Fourcaud, T. 2014. Tree stability under wind: simulating uprooting with root breakage using a finite element method, *Annals of botany* **114**(4), 695–709.

Zhang, X., Knappett, J.A., Leung, A.K., Ciantia, M.O., Liang, T., Nicoll, B.C. 2023. Centrifuge modelling of root–soil interaction of laterally loaded trees under different loading conditions, *Géotechnique* **73**(9), 766–780.

Zhu, J., Leung, A. K., Wang, Y. 2022. Modelling root–soil mechanical interaction considering root pull-out and breakage failure modes, *Plant and Soil* **480**(1), 675–701.

Zhu, J., Leung, A. K., Wang, Y. 2024. A computationally-efficient finite-element model for solving root–soil mechanical interaction of complex root system architectures, *Computers and Geotechnics* **174**, 106604.

Zhu, J., Leung, A. K., Knappett, J. A., Zhang, X., Wang, Y. 2025. A new root–soil interface contact model to simulate the overturning behaviour of root system architectures, *Acta Geotechnica*, 1–21.